Wave Propagation in the Split Hopkinson Pressure Bar

P. S. Follansbee

C. Frantz

Materials Science and Technology Division,
Los Alamos National Laboratory,
Los Alamos, NM 87545

Elastic wave propagation in the split Hopkinson pressure bar (SHPB) is discussed with an emphasis on the origin and nature of the oscillations that often trail the leading edge of the pressure wave. We show that in the conditions of the SHPB test the pressure bars vibrate in the fundamental mode and that elastic wave propagation can be fully described mathematically. Excellent agreement is found between experimental results and predictions of the mathematical treatment. This suggests that dispersion effects in the pressure bars can be removed from the strain gage records, which reduces the magnitude of the oscillations in the resulting stress strain curve.

1 Introduction

High-strain-rate mechanical testing is complicated by the effects of stress wave propagation. At strain rates above 10^3 s^{-1} it is difficult to achieve uniform loading conditions over the gage length of a standard tensile specimen because there may be insufficient time to dampen the often complex stress waves generated during the test. The complex geometry associated with grips, specimen design, screw threads, etc. makes analysis of stress wave propagation in such a test virtually intractable.

The split Hopkinson pressure bar (SHPB) has evolved into a useful high-rate test apparatus because the stress waves generated in long cylinders are relatively simple and are capable of precise analysis. In addition, specimen dimensions have been reduced significantly to minimize delays associated with stress wave propagation. Nevertheless, certain features of wave propagation in the SHPB complicate the interpretation of test results.

This paper describes the elastic wave phenomena that apply to the SHPB. In particular, we discuss the origin and details of the large amplitude oscillations which are noted in the strain gage records. It will become evident that the oscillations can be fully described mathematically. Furthermore, we show how stress wave dispersion can be removed from the strain gage records to give a more accurate representation of the stresses and strains within the deforming specimen.

Although a short summary of the SHPB will be given, knowledge of the basic operation and various methods of data reduction are assumed. For further description of the SHPB test technique, the reader is referred to the detailed reviews by Lindholm [1, 2].

1.1 Operation of the SHPB. Figure 1 is a schematic of the SHPB used in this investigation. The pressure wave is generated in the incident pressure bar by the impact of the striker bar, which is propelled at a specified velocity. The wave travels down the bar, is recorded at strain gage A (E_i), is partially reflected at the incident bar/specimen interface, and partially reflected at the specimen/output bar interface. Strain gage B on the output bar records the portion of the wave that has transmitted the specimen E_t, while strain gage A on the incident bar records that portion of the wave reflected at the incident bar/specimen interface E_r. From these strain gage measurements, the stress and strain in the specimen, which is sandwiched between the two pressure bars, can be computed as a function of time. The strain gage traces

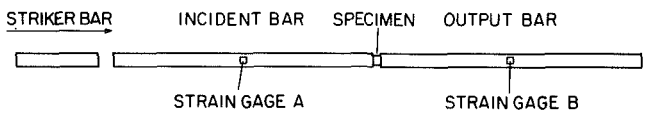

Fig. 1 Schematic of the split Hopkinson pressure bar test apparatus. The pressure bars used in these experiments were made from Maraging steel and were 1.22 m long by 9.2 mm in diameter. The specimens were typically 4.6 mm long by 7.6 mm in diameter.

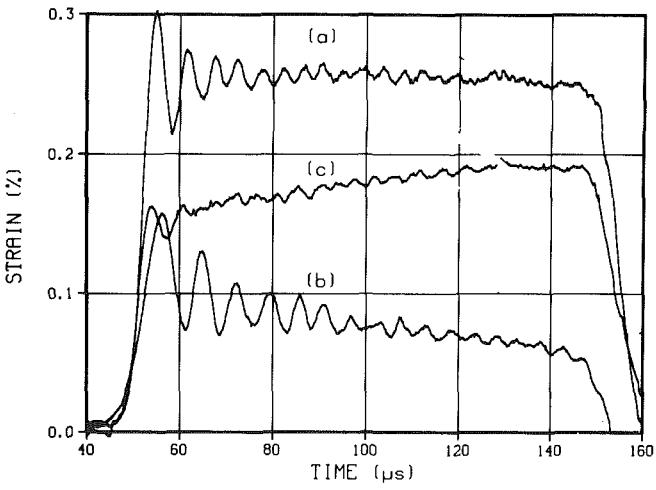

Fig. 2 Traces of the measured incident (*a*), inverted reflected (*b*), and transmitted (*c*) waves for a SHPB test on brass at a strain-rate of 1 × 10^3 s^{-1}. The reflected wave has been inverted here for ease of comparison.

Contributed by the Materials Division for publication in the JOURNAL OF ENGINEERING MATERIALS AND TECHNOLOGY. Manuscript received by the Materials Division, July 15, 1982.

of E_i, E_r, and E_t for a SHPB test on brass at a strain rate of 1×10^3 s^{-1} are shown in Fig. 2. Although E_i and E_t are compression waves, E_r is a tensile wave because the specimen is softer than the incident (and output) bars. Figure 2 shows the wave E_r inverted so that the amplitude and wavelength of the oscillations that trail the leading edge of the pressure waves can be compared more easily.

When the striker bar impacts the incident bar, a compressive, elastic pressure wave is set into motion in the incident bar. Near the impacted end, the nature of the pulse is highly complex because of: (*a*) friction conditions at the striker bar/incident bar interface, which may impose a radial constraint,[1] and (*b*) propagation of other types of elastic waves: for example, a spherical dilatational wave could propagate, but its amplitude decreases inversely with distance traveled along the incident bar. Farther than 10 bar diameters from the striker bar, however, end effects vanish [3, 4] and the vibrational behavior of an elastic bar excited by a longitudinal pulse is fully described by the equation of motion.

2 Solution of the Equation of Motion

The motion of a particle in the bar in response to any excitation is governed by the equation of motion. Pochhammer [5] and Chree [6] independently solved the equation of motion for the propagation of a sinusoidal wave in an infinitely long cylinder. The solution relates the propagation velocity C_p to the wavelength of the excitation Λ and is exact only for an infinitely long cylinder. For a cylinder whose length greatly exceeds its diameter, however, the errors are small [7]. In simplified form, the Pochhammer-Chree solution, which is also referred to as the frequency or dispersion equation, is written [3]

$$\frac{4\pi^2}{\Lambda^2}\left(\frac{\rho C_p{}^2}{\mu}-2\right)J_1(gR)\left[2\mu\frac{\partial^2 J_0(gR)}{\partial R^2} - \frac{\lambda\rho C_p{}^2 4\pi^2}{\Lambda^2(\lambda+2\mu)}J_0(gR)\right]+\frac{16\pi^2\mu}{\Lambda^2}\frac{\partial J_0(gR)}{\partial R}\frac{\partial J_1(hR)}{\partial R}=0, \quad (1)$$

where

$$g = \frac{\Lambda}{2\pi}\left[\frac{\rho C_p{}^2}{\lambda+2\mu}-1\right]^{0.5},$$

$$h = \frac{\Lambda}{2\pi}\left[\frac{\rho C_p{}^2}{\mu}-1\right]^{0.5},$$

$$\frac{\partial(\ )}{\partial R} = \frac{\partial(\ )}{\partial r}\Big]_{r=R},$$

J_0 is the Bessel function of the first kind of zero order, J_1 is the Bessel function of the first kind of order one, R is the radius of the bar, λ and μ are Lame's constants, and ρ is the density. Actually, an infinite number of solutions to the governing equation are possible, each of which corresponds to a unique mode of vibration. A direct analogy is found between the excitation or longitudinal vibration of a long cylinder and the vibration of a drum membrane. Although the boundary conditions differ, theoretically an infinite number of vibrational modes is possible in both cases in response to a longitudinal impact. The actual vibrational modes excited depend naturally on the particular configuration.

The Pochhammer-Chree solution for the first three vibrational modes is shown in Fig. 3 for a material with a Poisson's ratio of 0.29. It is evident that for all three modes the propagation (or phase) velocity decreases with decreasing wavelength; a high-frequency wave travels more slowly than a lower frequency wave.

In the SHPB test, the pressure bar is not excited by a pure sinusoid, but rather by a pulse that is composed of a spectrum of frequencies. In this case, the velocity of each frequency component can be determined independently. This is the basis of the appearance of the waves shown in Fig. 2. The higher frequency components of the pulse are traveling more slowly, and thus, lag behind the lower frequency components. A variation in phase velocity leads to the spreading, or dispersion, of an initially sharp pulse. The next step in the analysis is to identify which vibrational mode (or modes) has been excited by the specific conditions of the SHPB test.

3 Application of the Solution to the SHPB

A few investigators have attempted to identify the vibrational modes excited by the impact of a long cylinder. Curtis [8] excited a magnesium bar with a shock wave, and from strain gage records, was able to identify the contribution from vibrational modes as high as 6. Davies [9] made a thorough analysis of the response of a Hopkinson pressure bar to the impact of a projectile. In these experiments, displacements were measured with a condenser unit. Davies only found evidence of vibration of the fundamental mode (mode 1) and concluded that, in the conditions of impact with a Hopkinson bar, the "waves belong to the first mode of vibration." The difference between the Curtis and the Davis experiments is that, in the former, the amplitude of the stress wave reached only 0.31 MPa, which is more than two orders of magnitude less than that reached in the latter experiments. Given such a wide disparity in the excitation, it is not unreasonable to have differences in the vibrational response of the two bars.

The conditions in the SHPB test are comparable to those investigated by Davies, and, therefore, it might be expected that only waves of the first vibrational mode are excited. One way to verify this is to inspect E_i and E_r (Fig. 2) more carefully. If only the fundamental vibrational mode is excited, then it should be possible to apply the information given in

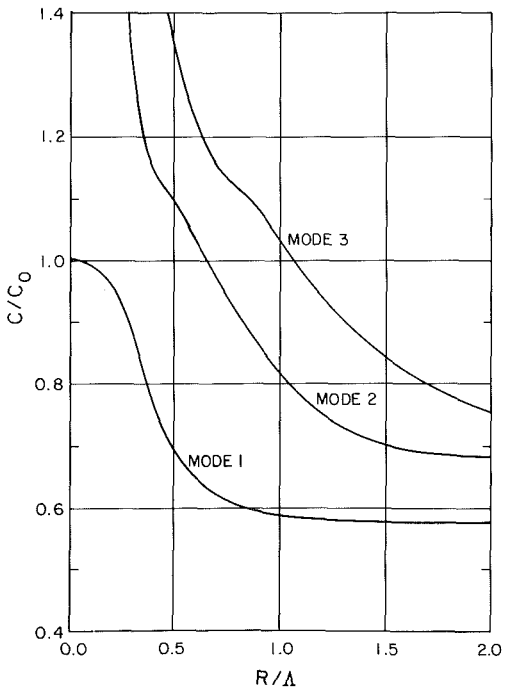

Fig. 3 Solution of the dispersion equation showing the variation of phase velocity with wavelength for the first three vibrational modes and for a material with Poisson's ratio of 0.29

[1] For ideal bars with flat ends, this only will be the case when the striker bar and incident bar are not identical in diameter or material. Since the standard practice is to round the end of the striker bar slightly to minimize misalignment as well as to increase the rise time of the pulse, friction at this interface may be a factor even for otherwise identical bars.

Fig. 3 to reconstruct these waveforms. Two comparisons are described. In the first, E_i is compared with that computed assuming a trapezoidal excitation at the striker bar/incident bar interface. In the second, E_i and E_r are corrected for dispersion to allow a comparison at the incident bar/specimen interface.

3.1 Mode 1 Response to a Trapezoidal Excitation. Davies [9] first outlined this procedure in 1948. The pulse initially excited in the incident bar is assumed to be trapezoidal. The Fourier transform of this waveform is

$$\frac{(u_z)_z}{(u_z)_0} = \frac{1}{2} - \frac{2}{\pi^2 s} \sum_{n=1,3,5,\ldots}^{\infty} \frac{(-1)^{\frac{(n-1)}{2}}}{n^2} \sin(\pi n s)\, \cos(n\omega_0 t), \tag{2}$$

where s and ω_0 are defined in Fig. 4. The Pochhammer-Chree solution tells us that the propagation velocity depends on the wavelength; thus, at a position z on the bar, the Fourier transform becomes

$$\frac{(u_z)_z}{(u_z)_0} = \frac{1}{2} - \frac{2}{\pi^2 s} \sum_{n=1,3,5,\ldots}^{\infty} \frac{(-1)^{\frac{(n-1)}{2}}}{n^2} \sin(\pi n s)\, \cos\left[n\omega_0\left(t' - \frac{z}{C_n}\right)\right], \tag{3}$$

where C_n is the propagation velocity of frequency component $n\omega_0$ and t' is measured from a time when all frequency components are in phase. It follows that

$$C_n = \frac{n\omega_0 \Lambda}{2\pi}, \tag{4}$$

where Λ is the wavelength of frequency component $n\omega_0$. Rearranging into a dimensionless form gives

$$\frac{Rn\omega_0}{C_0} = 2\pi \frac{C_n}{C_0} \frac{R}{\Lambda}. \tag{5}$$

Given R, C_0, and ω_0, the phase velocity corresponding to a given n can be derived from the information given in Fig. 3. The final step is to reconstruct the wave at z using equation (3).

These calculations were performed for the trapezoidal wave shown in Fig. 4 ($\omega_0 = 3.021 \times 10^4\ s^{-1}$ and $s = 0.014$) and for a bar radius of 4.6 mm and a longitudinal wave velocity C_0 equal to 4.83×10^3 m/s. Figure 5 shows the wave as reconstructed at the location of strain gage A ($z = 0.61$ m) along with the measured wave E_i. Although the oscillations trailing the leading edge of the pulse do not all correspond exactly in amplitude or location, the agreement between the predicted and measured waveforms is fairly close considering that the computed wave varies according to the assumed excitation.

Inspection of equation (3) indicates that the amplitude of the Fourier components does not change with time or distance traveled; only the phase angles change. The appearance of the large oscillations riding on the waves shown in Fig. 2 may suggest that some frequency components are growing in amplitude at the expense of others. It is important to emphasize that there is no physical means of such amplification in this problem. (Nor is there assumed to be any means of dampening in this elastic problem.) The appearance of the waves in Fig. 2 is strictly due to the variation of the propagation velocity with frequency, which leads to phase lags of the higher frequency Fourier components.

The agreement between the measured and predicted waveforms in Fig. 5 supports the contention that only the fundamental mode of vibration is excited in the pressure bar. A more conclusive test, however, would be to compare E_i and

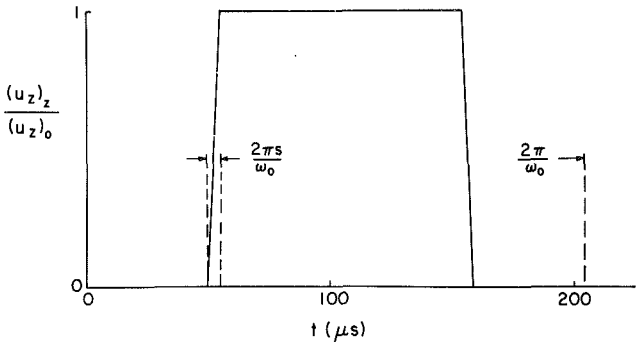

Fig. 4 Trapezoidal wave configuration

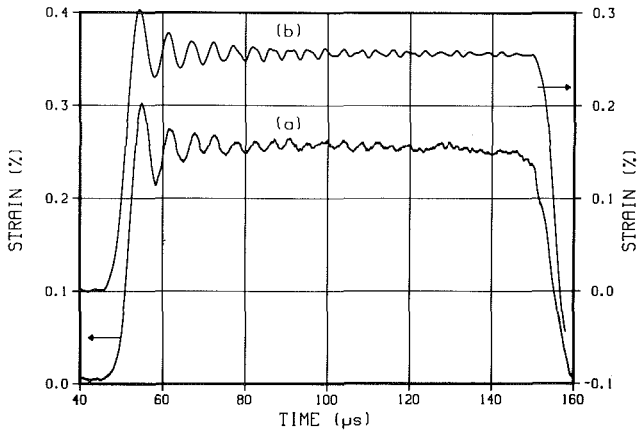

Fig. 5 Comparison of the incident wave measured at strain gage A (*a*) with the wave predicted assuming an initial trapezoidal excitation (*b*)

E_r after correcting for the effects of dispersion assuming only mode 1 vibrations. This comparison is described below.

3.2 Dispersion Correction for Mode 1 Vibrations. In the previous section, the dispersion correction for an assumed waveform was performed by first transforming the wave from the time domain to the frequency domain, then introducing the variation of phase velocity with wavelength, and finally converting back to the time domain. The identical procedure can be applied to correct any waveform for dispersion. One form of the Fourier transform of a wave $f(t)$ is written

$$f(t) = \frac{A_0}{2} + \sum_{n=1}^{\infty} D_n \cos(n\omega_0 t - \delta). \tag{6}$$

The phase angle δ is found by replacing t' in equation (3) with

$$t' = t + \frac{z}{C_0} \tag{7}$$

and simplifying to give

$$\delta = \frac{n\omega_0 z}{C_0}\left(\frac{C_0}{C_n} - 1\right). \tag{8}$$

Thus, the dispersion of any wave can be determined and accounted for by adjusting the phase angle according to

$$\delta = \delta_0 + \frac{n\omega_0 \Delta z}{C_0}\left(\frac{C_0}{C_n} - 1\right), \tag{9}$$

where

δ_0 is the phase angle at z_0, and
δ is the phase angle at $z = z_0 + \Delta z$.

As expected, the phase angle increases for a positive Δz. To illustrate the application of this equation, Fig. 6 shows the measured E_i (at A) along with the predicted wave recon-

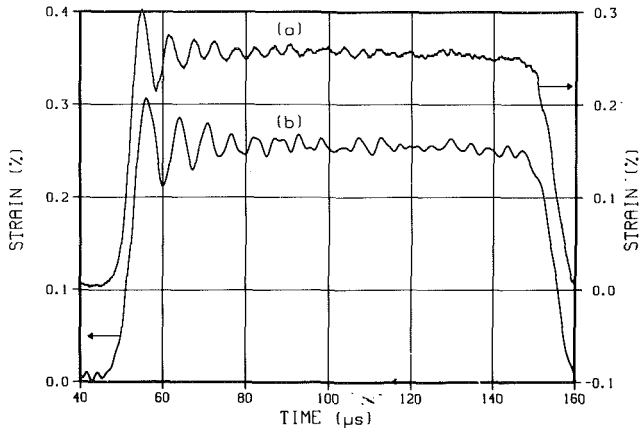

Fig. 6 Comparison of the incident wave measured at strain gage A (*a*) with the corresponding wave as predicted at the incident bar/specimen interface (*b*)

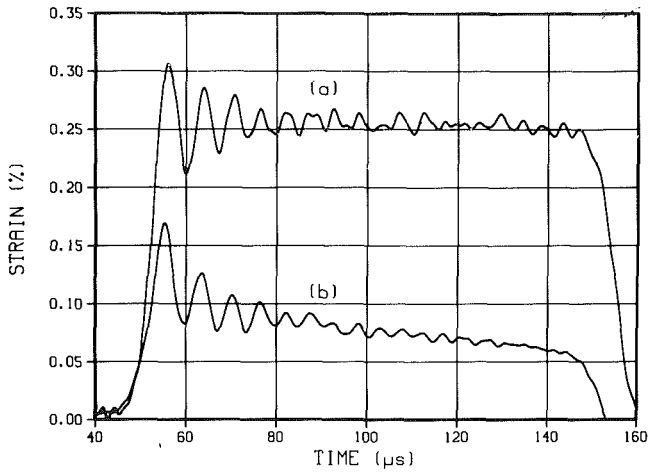

Fig. 7 Comparison of the incident wave (*b*) and inverted reflected wave (*b*) as predicted at the incident bar/specimen interface. The reflected wave has been inverted here for ease of comparison.

structed at the specimen/incident bar interface ($\Delta z = 0.61$ m). The dispersion correction in this case has effectively stretched the wave. The reflected wave can also be reconstructed at the specimen/incident bar interface. This requires that wave dispersion be removed ($\Delta z = -0.61$ m). The incident and reflected waves reconstructed at the specimen/incident bar interface are plotted together in Fig. 7. It is evident that, whereas the peaks and valleys in E_i and E_r did not correspond in time before the dispersion correction, there is now excellent correspondence. This agreement is conclusive evidence that it is mainly the fundamental mode of vibration which has been excited in the SHPB test, as was predicted by Davies. If significant contributions from other modes had been present, then the dispersion correction based on the phase velocity versus wavelength relationship for mode 1 vibrations would not have been as successful.

3.3 Radial Variation of the Longitudinal Stresses and Strains. One prediction of the full Pochhammer-Chree solution to the problem involving the propagation of elastic waves in an infinite bar is that the longitudinal stress and displacement will vary across the cross section. This variation is a function of the ratio of the bar radius to the wavelength, R/Λ; for $R/\Lambda << 1$, the longitudinal stress and displacement profiles are flat. For small wavelengths, however, the variation can be significant.

In these SHPB tests, the stress and strain in the deforming specimen are determined from strain gage measurements on the surface of the pressure bars. Thus, a significant radial variation of the longitudinal displacement will lead to gross errors in the estimated stress and strain. In addition, valid test requires a uniform stress state within the specimen. Davies [9] computed the ratio of the longitudinal displacement at the surface to that along the bar axis and from these calculations showed that, for $R/\Lambda < 0.10$, the displacement at the surface differs from that along the axis by less than 5 percent. Table 1 lists the amplitude of the Fourier components and values of R/Λ versus n for the wave E_i of Fig. 2. For the conditions of this experiment, R/Λ remains below 0.10 for $n < 22$ at which time the magnitude of the Fourier component has fallen to only ~ 2 percent of the highest magnitude component (A_0). Thus, for the conditions of the SHPB, the longitudinal displacement varies negligibly over the cross section. The same result applies to the radial variation of the longitudinal stress, which leads to the conclusion that the SHPB configuration shown in Fig. 1 yields a one-dimensional stress state and that the strain gage records are reliable measurements of the displacements within the bars.

The next step in the analysis is to see how this new understanding of elastic wave propagation can be used to advantage in the SHPB test.

Table 1 Fourier series coefficients and values of R/Λ for E_i

n	$\frac{R}{\Lambda}$	$\frac{D(n)}{A_0}$
1	0.0046	0.634
2	0.0092	0.0066
3	0.0138	0.201
4	0.0184	0.0082
5	0.0230	0.1103
6	0.0276	0.0098
7	0.0321	0.0761
8	0.0367	0.0100
9	0.0413	0.0560
10	0.0459	0.0087
11	0.0505	0.0466
12	0.0551	0.0111
13	0.0597	0.0364
14	0.0644	0.0116
15	0.0690	0.0284
16	0.0736	0.0112
17	0.0782	0.0230
18	0.0829	0.0095
19	0.0875	0.0183
20	0.0922	0.0119
21	0.0968	0.0159
22	0.1015	0.0114
23	0.1062	0.0146
24	0.1109	0.0131
25	0.1156	0.0144
26	0.1203	0.0125
27	0.1251	0.0085
28	0.1299	0.0131
29	0.1347	0.0105
30	0.1395	0.0110
31	0.1444	0.0068
32	0.1493	0.0084
33	0.1542	0.0076
34	0.1592	0.0093
35	0.1642	0.0071

3.4 Incorporating the Dispersion Correction Into the SHPB Test. The strain and strain rate in the deforming specimen are related to the strain gage records by [1]

$$\epsilon = \frac{u_1 - u_2}{l_0} = \frac{C_0}{l_0}\int_0^t (E_i - E_r - E_t)\,dt \text{ and} \qquad (10)$$

$$\frac{d\epsilon}{dt} = \frac{V_1 - V_2}{l_0} = \frac{C_0}{l_0}(E_i - E_r - E_t),$$

where compressive strain is defined as positive, u_1 and u_2 are the displacements at the specimen/incident bar and

specimen/output bar interfaces, V_1 and V_2 are the velocities at the specimen/incident bar and specimen/output bar interfaces, and l_0 is the length of the specimen. The stress within the specimen is

$$\sigma = \frac{P_1 + P_2}{2\ S_0} = \frac{E\ S_b}{2\ S_0}\ (E_i + E_r + E_t), \tag{11}$$

where P_1 and P_2 are the forces at the specimen/incident bar and specimen/output bar interfaces, E is Young's modulus, S_b is the cross-sectional area of the pressure bar, and S_0 is the cross-sectional area of the specimen. At the incident bar/specimen interface (1) and the specimen/output bar interface (2),

$$\sigma_1 = \sigma_2,$$

which implies that

$$E_i + E_r = E_t, \tag{12}$$

so that the expressions for the strain, strain rate, and stress in the specimen simplify to

$$\epsilon = \frac{-2\ C_0}{l_0} \int_0^t E_r\ dt,$$

$$\frac{d\epsilon}{dt} = \frac{-2\ C_0}{l_0} E_r, \text{ and} \tag{13}$$

$$\sigma = \frac{E\ S_b\ E_t}{S_0}.$$

The above expressions indicate that the stress within the deforming specimen is directly related to the amplitude of the transmitted wave and that the strain within the specimen is related to the time integral of the amplitude of the reflected wave. These equations are strickly valid only at the specimen interface; yet E_r and E_t are not measured at this interface. Thus to apply equations (13), the reflected and transmitted waves should be corrected for any dispersion which occurs during propagation from the specimen interface to the location of the strain gages. If these corrections are not performed, the resulting stress strain curve may exhibit oscillations that are not representative of the true specimen behavior.

The errors introduced by neglecting dispersion are illustrated in Fig. 8 which compares the stress strain curves computed using equations (13) and E_r and E_t with and without the dispersion correction. The curve using the corrected strain gage records is much smoother (the oscillations are less apparent), particularly in the yield region, than that using the raw data. Two other examples of the effect of the dispersion correction on the measured stress strain curves of OFE copper and iridium are shown in Figs. 9 and 10. Both figures indicate that the dispersion correction has a large effect, again, particularly in the yield region. It is also evident that the correction is not perfect. For the case of iridium (Fig. 10) a rather large oscillation remains at a strain of 0.015. The origin of this problem is unclear; perhaps too few terms were used in the Fourier transform (49 terms were computed). It is also possible that the oscillation is due to a higher order vibrational mode which has not been considered. For copper (Fig. 9) the dispersion correction has yielded a slight increase in the amplitude of the oscillations in the high strain region. We have found that this problem is related to complications in the unloading portion of the stress wave. Even with these imperfections, the stress strain curves constructed using the dispersion correction are considerably smoother and offer much better information in the yield region that those constructed using the raw data. Thus we conclude that the dispersion correction should be incorporated into the SHPB data reduction procedure.

A correction for wave dispersion has not appeared in most

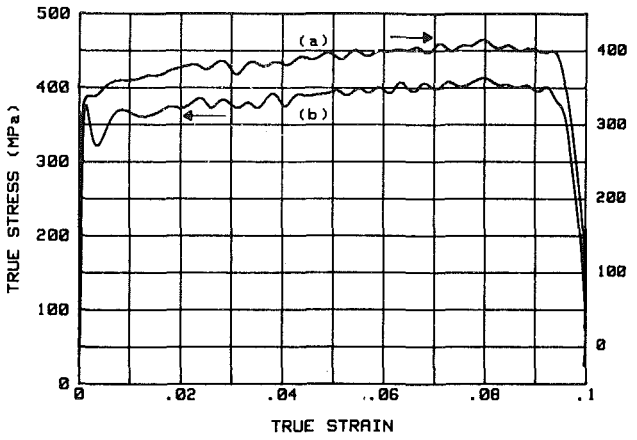

Fig. 8 Stress strain curves for brass constructed with (*a*) and without (*b*) the dispersion correction

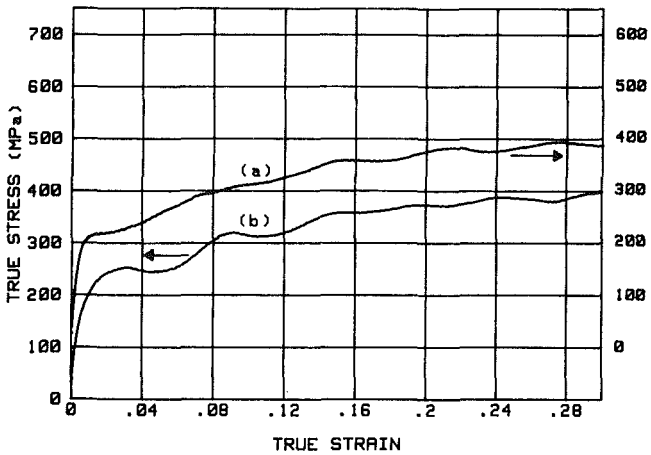

Fig. 9 Stress strain curves for work hardened OFE copper at a strain rate of $7 \times 10^3\ s^{-1}$ constructed with (*a*) and without (*b*) the dispersion correction

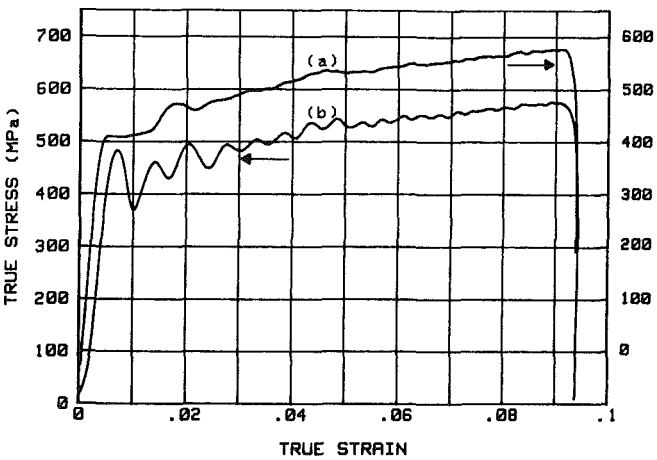

Fig. 10 Stress strain curves for annealed iridium at a strain rate of $1.5 \times 10^3\ s^{-1}$ constructed with (*a*) and without (*b*) the dispersion correction

of the previous investigations of high-rate behavior using the SHPB. Davies and Hunter [10] derived an approximate correction assuming an initial discontinuous or step excitation. Their correction results in an expansion of the time scale by a factor β and, for the assumed excitation, is an accurate description of the dispersion of the leading edge of

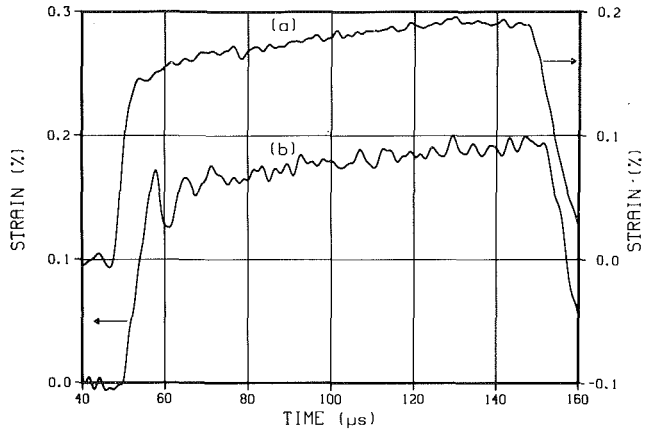

Fig. 11 Comparison of the transmitted wave as predicted at the specimen/output bar interface (*a*) with that predicted at the incident bar/specimen interface from equation (12) (*b*).

the incident wave. As the authors point out, however, the application of the same correction factor to the reflected and transmitted waves strictly requires that the shape of these waves be similar to that of the input profile. Other investigators have assumed that the displacement time records measured far from the specimen interface are equivalent to those at the interfaces. In making this assumption, these investigators have either argued that dispersion effects are negligible or that they are minimized by placing the strain gages equidistant from the interfaces. Neither argument is valid for the conditions in which the waves shown in Fig. 2 and the stress strain curves in Figs. 8–10 were measured.

Application of the dispersion correction has successfully reduced the amplitude of, but has not eliminated, the oscillations in the measured stress strain curve. It would appear, then, that a real oscillation in the strain rate is transmitted to the specimen. To this point, we have limited the discussion to the elastic behavior of the pressure bars. Now questions arise concerning the wave propagation in the plastically deforming specimen, which is far more difficult to analyze. Bertholf and Karnes [11, 12] have investigated the stress wave propagation in the SHPB test using a two-dimensional, finite-difference, elastic-plastic, computer code. Using this code, these authors have noted that the oscillations, which can be quite large in the incident and reflected waves, are rapidly dampened in the deforming specimen. This can be illustrated by comparing the wave transmitted at the incident bar/specimen interface, which can be computed from equation (12), with that transmitted at the specimen/output bar interface. The comparison of these two waves in Fig. 11 indicates that the wave transmitted into the specimen contains much larger oscillations than that transmitted into the output bar. This experimental result agrees with the computations of Bertholf and Karnes. Furthermore, the observed dampening of the oscillations in the plastically deforming specimen suggests that it is more accurate to use the transmitted wave measured on the output bar and adjusted to the specimen interface in equations (13) than it would be to use the computed wave transmitted at the incident bar/specimen interface. Further analysis of wave propagation within the deforming specimen would require the application of a numerical method similar to that used by Bertholf and Karnes.

4 Summary

This paper has described elastic wave propagation in the SHPB. The important feature of the SHPB configuration shown in Fig. 1 is that the bars respond to the impact of the striker bar by vibrating in the fundamental mode. This has been demonstrated by the agreement between the waveform measured at a given location on the bar with that computed at the same location assuming a trapezoidal excitation. Even more convincing proof resulted from the similarities between the waves E_i and E_r when corrected for dispersion so that they corresponded to the same bar location. Satisfied that in these experiments the fundamental mode is indeed the primary mode of vibration, it becomes possible to apply the mathematical solution to the equation of motion to correct for wave dispersion in the SHPB test. The dispersion correction leads to a smoother stress strain curve than obtained with the raw strain gage data. The procedure for making this correction requires (*a*) a Fourier transform of the wave measured at any location z_0, (*b*) an operation on the individual Fourier components to correct for the variation in phase velocity with wavelength, and (*c*) the reconstruction of the wave at $z = z_0 + \Delta z$. Although the conclusions reached in this investigation strictly apply only to the SHPB configuration shown in Fig. 1, it should be possible to apply the same methodology to analyze wave propagation in any SHPB test configuration.

Elastic wave behavior in the pressure bars now appears to be well understood; wave propagation in the plastically deforming specimen, however, remains a question. One result of plastic deformation is that it leads to a dampening of oscillations in the pressure wave. The analysis of this effect and the prediction of the time required for uniform conditions to be attained in the deforming specimen is far more difficult mathematically and requires the application of numerical procedures.

References

1 Lindholm, U. S., "Some Experiments with the Split Hopkinson Pressure Bar," *Journal of the Mechanics and Physics of Solids*, Vol. 12, 1964, pp. 317–335.

2 Lindholm, U. S., "High Strain Rate Tests," in *Measurement of Mechanical Properties*, Vol. V, Part 1, R. F. Bunshah, Ed., Interscience, New York, 1971, Chap. 4, pp. 199–271.

3 Wasley, R. J., *Stress Wave Propagation in Solids*, Marcel Dekker, New York, 1973.

4 Yeung Wye Kong, Y. C. T., Parsons, B., and Cole, B. N., "The Dispersive Behavior of a Hopkinson Pressure Bar in Material Property Tests," in *Mechanical Properties at High Rates of Strain*, Institute of Physics Conference Series No. 21, 1974, pp. 33–47.

5 Pochhammer, L., "On the Propagation Velocities of Small Oscillations in an Unlimited Isotropic Circular Cylinder," *Journal fur die Reine und Angewandte Mathematik*, Vol. 81, 1876, pp. 324–326.

6 Chree, C., "The Equations of an Isotropic Elastic Solid in Polar and Cylindrical Coordinates, Their Solutions and Applications," Cambridge Philosophical Society, *Transactions*, Vol. 14, 1889, pp. 250–369.

7 Kolsky, H., *Stress Waves in Solids*, Dover Publications, New York, 1963.

8 Curtis, C. W., "Propagation of an Elastic Pulse in a Semi-Infinite Bar," in *International Symposium on Stress Wave Propagation in Materials*, N. Davids, Ed., Interscience, New York, 1960, pp. 15–43.

9 Davies, R. M., "A Critical Study of the Hopkinson Pressure Bar," *Philosophical Transactions A*, Vol. 240, 1948, pp. 375–457.

10 Davies, E. D. H., and Hunter, S. C., "The Dynamic Compression Testing of Solids by the Method of the Split Hopkinson Pressure Bar," *Journal of the Mechanics and Physics of Solids*, Vol. 11, 1963, pp. 155–178.

11 Bertholf, L. D., "Feasibility of Two-Dimensional Numerical Analysis of the Split Hopkinson Pressure Bar System," ASME *Journal of Applied Mechanics*, Vol. 41, 1974, pp. 137–144.

12 Bertholf, L. D., and Karnes, C. H., "Two-Dimensional Analysis of the Split Hopkinson Pressure Bar System," *Journal of the Mechanics and Physics of Solids*, Vol. 23, 1975, pp. 1–19.